Raman Spectrum of Cubic ZnS

W. G. NILSEN
Bell Telephone Laboratories, Murray Hill, New Jersey 07974
(Received 3 September 1968; revised manuscript received 7 February 1969)

We present a detailed study of the first- and second-order Raman effect in cubic ZnS using both 4880 and 5145 Å excitation. Our primary interest is to determine to what extent information on lattice dynamics can be extracted from Raman studies in a case where the crystal structure is relatively simple. Aside from interpreting the observed spectra and determining the energies of the phonon branches at the Brillouin-zone center and boundary, the study emphasizes two things. First, we examine experimentally the relation between first-order Raman intensities and the linear electro-optic effect. We find that the linear electro-optic constant derived from the absolute Raman intensities of the longitudinal- (LO) and transverse- (TO) optic modes agrees quite well with the constant obtained from direct measurement. This close agreement is particularly significant in the zinc-blende structure, since only one electro-optic constant and two optical modes are involved in the comparison. Also, it provides experimental evidence that the macroscopic, and not the local, electric field caused by the polar phonons should be used in calculations involving semiconducting crystals. Second, emphasis was also placed on comparing the observed selection rules or polarization properties of the second-order Raman effect with that predicted at the two most important or highest-symmetry critical points (X and L) on the Brillouin-zone boundary. The agreement between observed and calculated selection rules is quite good, although in some cases, certain polarization characteristics which are allowed by symmetry are not detected. Also, some evidence of two-phonon scattering from other points in the Brillouin zone is found. The polarization properties of single-crystal Raman spectra are more conveniently discussed in terms of the irreducible representations of the polarizability, rather than depolarized spectra or depolarization ratios which apply more directly to liquid or polycrystalline samples. The observed and calculated selection rules for second-order Raman scattering are compared in detail, using these polarizability representations. The LO and TO phonon energies are 271 and 352 cm^{-1} at the zone center and 306 and 333 cm^{-1} at the zone boundary, and the TA and LA energies are 88 and 110 cm^{-1} at the boundary.

INTRODUCTION

CRYSTALS with the zinc-blende structure have been the subject of extensive study for some time. There are several reasons for the interest in this particular crystal structure. First, it is amongst the simplest structures found in nature for a polar crystal lacking inversion symmetry. For this reason, theoretical calculations are more easily made and experimental results more easily interpreted with the zinc-blende structure than with more complex structures. Second, a large number of semiconducting and insulating substances have this crystal structure which makes the results of such investigations of more general interest.

The present paper presents a study of the first- and second-order Raman spectrum of cubic ZnS. Our primary objective was to interpret the second-order spectrum and compare these experimental results with the selection rules derived for the zinc-blende structure. It seemed that in this simple case, some judgment could be made as to the value of the second-order Raman effect in obtaining information about the lattice dynamics of a particular crystal. Our interest in the first-order spectrum was to compare the relative scattering intensities of the transverse-optic (TO) and longitudinal-optic (LO) modes with that predicted by theory from the linear electro-optic effect.

The Raman spectrum of cubic ZnS has been examined previously by Couture-Mathieu and Mathieu.[1] They found the LO and TO modes at 349 and 274 cm^{-1} but did not detect any second-order Raman spectra. Poulet[2,3] used these results to test the Lyddane-Sachs-Teller equation and found that this relation is closely obeyed in cubic ZnS.

The lattice dynamics of cubic ZnS has also been investigated by infrared techniques principally by Deutsch.[4] He examines the infrared absorption in the region from one to 24 μ at several different temperatures from about 8–400°K. He also interprets the spectrum in terms of two- and three-phonon absorption but the author admits that the interpretation is not unique. Johnson[5] gives an alternative interpretation of Deutsch's data but once again considerable ambiguity exists. In both cases, the derived phonon energies are not in agreement with the present work. Marshall and Mitra[6] give two alternative interpretations of Deutsch's data in terms of phonon energies at the zone boundary, but again the agreement with our work is not good, although better than with Deutsch's and Johnson's interpretations.

CRYSTAL STRUCTURE AND SELECTION RULES

As mentioned above, cubic ZnS crystallizes in the zinc-blende structure. This structure is most easily visualized as two face-centered cubic lattices displaced

[1] L. Coutre-Mathieu and J. P. Mathieu, Compt. Rend. **236**, 371 (1953); J. P. Mathieu and L. Couture-Mathieu, *ibid.* **233**, 32 (1951).

[2] H. Poulet, Compt. Rend. **236**, 373 (1953).
[3] H. Poulet, Ann. Phys. (Paris) **10**, 908 (1955).
[4] T. Deutsch, in *Proceedings of the International Conference on the Physics of Semiconductors, Exeter* (The Institute of Physics and the Physical Society, London, 1962), p. 505.
[5] F. A. Johnson, Progr. Semicond. **9**, 179 (1965).
[6] R. Marshall and S. S. Mitra, Phys. Rev. **134**, A1019 (1964).

from one another by one-quarter of a body diagonal. One lattice consists of zinc atoms and the other of sulphur atoms. The space group of the cubic unit cell is $F\bar{4}3m(T_d^2)$ and the cell contains four formula weights of ZnS. Although the zinc blende structure is most easily visualized in this manner, the primitive unit cell is trigonal and contains only one formula weight of ZnS. The base vectors for this unit cell join the origin to the three closest face-centered atoms in the cubic unit cell. We continue to discuss the zinc-blende structure in terms of the cubic unit cell but recoginze that only one zinc atom and one sulphur atom are unique; the other atoms in the cubic cell are connected by primitive translations. The structure has six degrees of freedom, three acoustic and three optical.

First-Order Raman Effect

In the first-order Raman effect, momentum conservation restricts the range of phonon wave vectors that can participate in the scattering process to those very near the Brillouin-zone center. Under these conditions, the phonon wave vector can be regarded as zero. Thus, only the point group of the unit cell (rather than the full space group of the crystal) need be considered in deriving the symmetry species of the vibrational modes and the selection rules for Raman activity. For the zinc-blende structure at the zone center, both acoustic and optical modes are triply degenerate and have symmetry species $\Gamma_{15}(F_2)$.

In addition to crystal symmetry considerations, Poulet[3] has shown that in polar crystals the macroscopic electric field associated with the LO mode tends to make its energy greater than the energy of the TO mode. This effect not only removes part of the degeneracy of the optical $\Gamma_{15}(F_2)$ mode, but also affects the intensities of the TO and LO modes. We shall discuss these effects in more detail in the Discussion section. The selection rules remain unaltered provided proper account is taken of the polarization characteristics of the phonon being created or destroyed.

These selection rules are most easily derived using a procedure due to Poulet.[3] We adapt rectangular coordinates X, Y, Z for our laboratory system with the incident light directed along Z and the scattered light detected along X. Since momentum is conserved in the Raman effect, the wave vector of the phonon created (or destroyed) in the process lies in the XZ plane and makes a 45° angle with the X and Z coordinate axes. In cubic crystals, the triply degenerate F-type vibrations are characterized by three normal coordinates. In deriving the differentiated polarizability tensors given, for example, by Loudon,[7] these normal coordinates are taken to be along the base vectors of the cubic unit cell. We wish to transform these tensors so that one normal coordinate, q_l, is parallel to the wave vector of the phonon and the other two, q_{t1}, and q_{t2}, are perpendicular to this wave vector. In this way, we obtain tensors which apply to purely longitudinal and transverse phonons. These tensors are then transformed into the laboratory coordinate system. In order to obtain quantities proportional to the Raman intensity, the elements of the differentiated polarizability tensors are squared and the results for the degenerate TO modes are added together. For convenience, we call these quantities intensity matrices in agreement with Poulet. The results for ZnS crystals oriented so that the $\langle 100\rangle$ directions are parallel to X, Y, Z laboratory coordinate system are

$$\theta_{\mathrm{LO}}(100)=\epsilon_F^2\begin{pmatrix}0 & \frac{1}{2} & 0\\ \frac{1}{2} & 0 & \frac{1}{2}\\ 0 & \frac{1}{2} & 0\end{pmatrix};\qquad \theta_{\mathrm{TO}}(100)=\epsilon_F^2\begin{pmatrix}0 & \frac{1}{2} & 1\\ \frac{1}{2} & 0 & \frac{1}{2}\\ 1 & \frac{1}{2} & 0\end{pmatrix}.$$

Here, θ_{LO} and θ_{TO} refer to LO and TO modes, and ϵ_F is the electric-field intensity of the incident light. For a crystal oriented so that a $\langle 100\rangle$ direction is along Y and two $\langle 110\rangle$ directions are along X and Z, the intensity matrices became

$$\theta_{\mathrm{LO}}(110)=\epsilon_F^2\begin{pmatrix}0 & \frac{1}{2} & 0\\ \frac{1}{2} & 0 & \frac{1}{2}\\ 0 & \frac{1}{2} & 0\end{pmatrix};\qquad \theta_{\mathrm{TO}}(110)=\epsilon_F^2\begin{pmatrix}1 & \frac{1}{2} & 0\\ \frac{1}{2} & 0 & \frac{1}{2}\\ 0 & \frac{1}{2} & 1\end{pmatrix}.$$

These matrices yield the polarization properties of the Raman effect for given crystal orientations. We emphasize again that even though θ_{LO} and θ_{TO} are equal for particular polarizations of incident and scattered light, the Raman intensities of LO and TO modes need not be the same since other terms in the expression for these intensities are different for the two modes. We show this more explicitly in the Discussion section in connection with deriving the linear electro-optic constant from the Raman intensities of the LO and TO modes. In nonpolar crystals, the intensity matrix for F-symmetry optical modes is the sum of θ_{LO} and θ_{TO}.

Second-Order Raman Effect

In the second-order Raman effect, the selection rules are more difficult to determine and use to interpret the observed spectra. The basic reason for this is that momentum conservation now involves two phonons so that the scattering process need not originate near the Brillouin-zone center as in the first-order effect. Indeed, since the density of two-phonon states tends to become greater for larger phonon wave vectors, it is likely that most, if not all, of the observed second-order scattering originates near the Brillouin-zone boundary. The phonon wave vectors in this part of the zone are much larger than the wave vector of the exciting radiation used in our experiments. Thus, the wave vectors of the two phonons taking part in the scattering event should have nearly equal magnitudes but be pointing in opposite directions. In other words, the two phonons created or destroyed in the second-order

[7] R. Loudon, Advan. Phys. 13, 423 (1964).

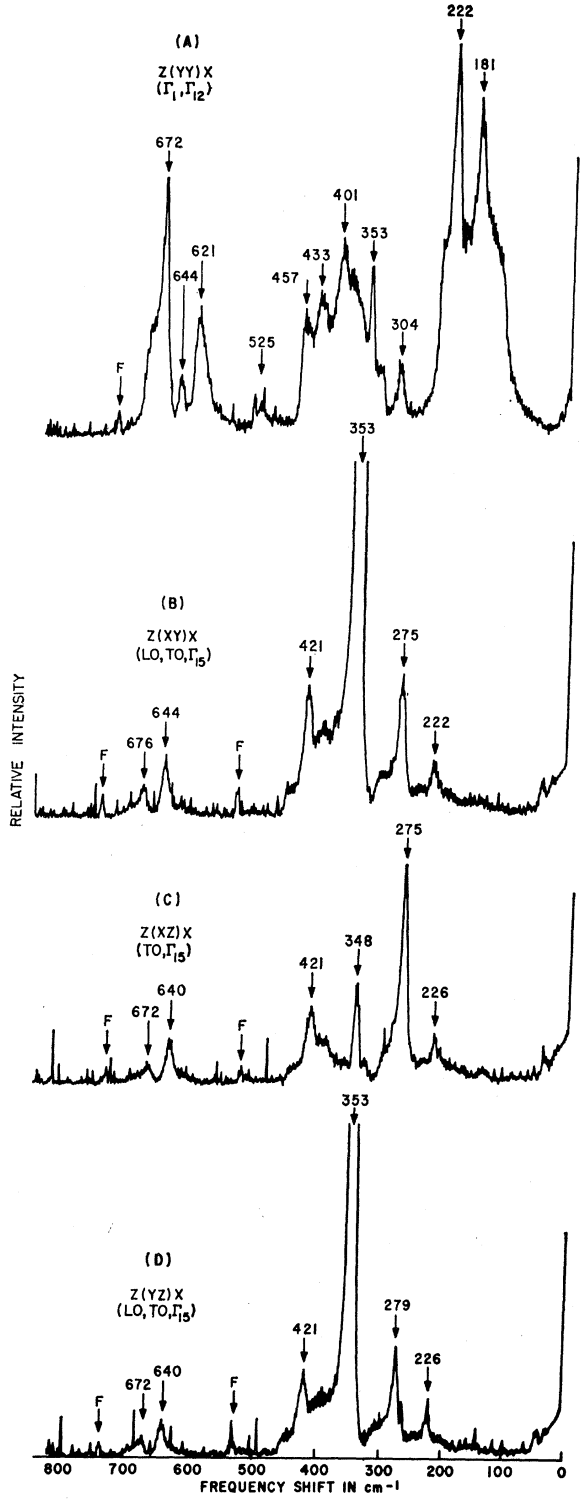

FIG. 1. Right-angle Raman scattering of cubic ZnS at room temperature and 4880-Å excitation. The three ⟨100⟩ crystallographic directions are along the X, Y, Z laboratory directions. The first and last letters in the notation $Z(YY)X$ indicate the direction of propagation for the incident and scattered light, respectively; the first and last letters inside the parentheses indicate the polarization directions of incident and scattered light, respectively. Also indicated with each spectrum is which (LO or TO) first-order Raman lines and which irreducible representations of the polarizability are measured.

Raman effect originate from near the same symmetry point in the Brillouin zone. Also, the combined density of states tends to become very large at the critical points on the zone boundary. For this reason, we attempt to interpret our results in terms of scattering by phonons at the X, L, and W critical points on the Brillouin-zone boundary. It should be realized, however, that scattering from other points in the zone undoubtedly contributed same background to the second-order spectra. Also, scattering from the three above critical points probably overlap one another in the Raman spectra and it is difficult to separate out contributions from the individual critical points.

The second-order Raman selection rules have been derived by Birman[8,9] for the zinc-blende structure. Here, we shall only outline that part of the calculation concerning the critical points of interest to us. First, we determine the symmetry species of the crystal vibrations at the three critical points X, L, and W. At point X, the point group of the space group[10] is D_{2d}, and the crystal vibrations have symmetry species[11] $X_1+X_3+2X_5$. We associate the doubly degenerate X_5 species with the TO and TA modes and the species X_1 and X_3 with the LA and LO modes. The exact association between the X_1 and X_3 symmetry species and the LA and LO vibrational modes is not known. At point L, the point group is C_{3v} and the species is $2L_1+2L_3$. The L_3 species are doubly degenerate and we associate these with the TA and TO modes; L_1 goes with the LA and LO modes. For the X and L points, only four distinct branches are present because of the degeneracy in the transverse-polarized modes. Also, the polarizations are well defined; that is, the vibrations are either pure transverse or pure longitudinal.

At critical point W, the point group is S_4 and the representation of the atomic displacements reduces to $W_1+2W_2+2W_4+W_3$. Only one degeneracy exists, symmetry species W_3 and W_4 are degenerate by time-reversal invariance. Also, these modes can no longer be divided into purely longitudinal or transverse polarized modes at critical point W.

The symmetry properties of the two-phonon states at these critical points can be derived from the reducible direct-product representation of the corresponding one-phonon states. The ordinary Kronecker square representation $\Gamma^{(j)}\times\Gamma^{(j')}$ is used for combination states and a symmetrized Kronecker square $[\Gamma^{(j)}]_2$ for overtone states. The procedure for obtaining these repre-

[8] R. L. Birman, Phys. Rev. **127**, 1093 (1962).
[9] J. L. Birman, Phys. Rev. **131**, 1489 (1963).
[10] G. F. Koster, in *Solid State Physics*, edited by F. Seitz and D. Turnbull (Academic Press Inc., New York, 1957), Vol. 5, p. 173.
[11] H. Poulet, J. Phys. (Paris) **26**, 684 (1965); see also R. H. Parmenter, Phys. Rev. **100**, 573 (1955).

sentations and the coupling coefficients for reducing the representations are given by Birman[8] for the zinc-blende structure. For crystal structures with T_d point group, the polarizability tensor transforms as $\Gamma_1+\Gamma_{12}+\Gamma_{15}$ where the individual Raman tensors associated with each of these irreducible representations are given by Loudon[7] under the labels A_1, E, and $F_2(x,y,z)$, respectively. If in the reduction of the direct-product representations, the coefficient of one or more of the irreducible representations Γ_1, Γ_{12}, or Γ_{15} is nonzero, then the transitions from the ground state to the corresponding two-phonon state is Raman allowed. Birman[8] finds that in cubic ZnS, all possible two-phonon combinations and overtones are Raman allowed at the critical points X, L, and W. In addition, he regards the scattered radiation as depolarized if Γ_1 is not contained in the direct product representation and finds that this is true for combination bands originating from different one-phonon irreducible representations. While this method of describing the polarization properties of the Raman effect is convenient for providing a general picture of the observed spectra, it applies mostly to liquids and polycrystalline samples, and tends to obscure much of the information which can be obtained from single-crystal samples. We also agree with Kleinman[12] that the concept of depolarization ratios is not a suitable way of describing polarization effects in single-crystal Raman spectra.

For the above reasons, we choose to discuss the second-order Raman spectra in terms of the actual irreducible representations of the polarizability rather than depolarized spectra or depolarization ratios. For example, the calculated selection rules or polarization properties of the second-order Raman spectra are given in Table I in terms of the actual irreducible representations of the polarizability which are contained in the reduction of the direct product representations of the two-phonon states.

With regard to the observed spectra, we determine which irreducible representations of the polarizability are present in each peak. To facilitate this, we derive for the two crystal orientations examined in this study the scattering matrices belonging to the irreducible representations of the polarizability appropriate for the T_d point group. These scattering matrices are derived in much the same way as for the TO and LO modes at the zone center. First, the scattering tensors corresponding to the three irreducible representations are transformed from the crystal orientation under examination into the laboratory coordinate system. Second, the individual terms in the transformed tensor are squared to give quantities proportional to the Raman scattering intensity. For the Γ_1 (or A_1) irreducible representation, we obtain

$$\Gamma_1(100)=a^2\begin{bmatrix}1&0&0\\0&1&0\\0&0&1\end{bmatrix};\quad \Gamma_1(110)=a^2\begin{bmatrix}1&0&0\\0&1&0\\0&0&1\end{bmatrix}.$$

[12] L. Kleinman, Solid State Commun. 3, 47 (1965).

TABLE I. Raman-allowed two-phonon process in zinc blende.

Species	Polarization characteristics	Type
$[X_5]_2$	$\Gamma_1+2\Gamma_{12}+\Gamma_{15}$	2 TO; 2 TA
$[X_1]_2$	$\Gamma_1+\Gamma_{12}$	2 LO; 2 LA
$[X_3]_2$	$\Gamma_1+\Gamma_{12}$	
$X_5\times X_1$	Γ_{15}	TO+LO; TO+LA
$X_5\times X_3$	Γ_{15}	TA+LO; TA+LA
$X_5\times X_5$	$\Gamma_1+2\Gamma_{12}+\Gamma_{15}$	TO+TA
$X_3\times X_1$	Γ_{15}	LO+LA
$[L_3]_2$	$\Gamma_1+\Gamma_{12}$	2 TO; 2 TA
$[L_1]_2$	$\Gamma_1+\Gamma_{15}$	2 LO; 2 LA
$L_3\times L_1$	$\Gamma_{12}+\Gamma_{15}$	TO+LO; TO+LA; TA+LO; TA+LA
$L_3\times L_3$	$\Gamma_1+\Gamma_{12}+2\Gamma_{15}$	TO+TA
$L_1\times L_1$	$\Gamma_1+\Gamma_{15}$	LO+LA
$[W_i]_2$	$\Gamma_1+\Gamma_{12}$	
$W_i\times W_j$	$\Gamma_1+\Gamma_{12}$ if $i=j$ no Γ_1 if $i\neq j$	a

[a] The vibrational modes cannot be divided into purely transverse polarized and purely longitudinal polarized at the critical point W in the zinc-blende structure.

Here, $\Gamma_1(100)$ refers to the crystal orientation in which the $\langle 100\rangle$ directions lie along the X, Y, Z coordinate axes, and $\Gamma_1(110)$ to that in which $\langle 110\rangle$ crystallographic directions are along X and Z but a $\langle 100\rangle$ direction is along Y. Spectra from the first crystallographic orientation is given in Fig. 1, the second orientation in Fig. 2. The corresponding scattering matrices for Γ_{12} (or E) are

$$\Gamma_{12}(100)=b^2\begin{bmatrix}4&0&0\\0&4&0\\0&0&4\end{bmatrix};\quad \Gamma_{12}(110)=b^2\begin{bmatrix}1&0&3\\0&4&0\\3&0&1\end{bmatrix}.$$

For Γ_{15} (or F), we have

$$\Gamma_{15}(100)=d^2\begin{bmatrix}0&1&1\\1&0&1\\1&1&0\end{bmatrix};\quad \Gamma_{15}(110)=d^2\begin{bmatrix}1&1&0\\1&0&1\\0&1&1\end{bmatrix}.$$

As noted above, the Γ_{15} matrices for each crystal orientation may be obtained from the sum of θ_{LO} and θ_{TO} given earlier in this section for the first-order Raman spectra.

By use of these matrices and the spectra in Figs. 1 and 2, the contributions from the individual irreducible representations can be obtained. The Γ_{12} and Γ_{15} polarizability representations can be measured directly by suitable arrangement of laser and scattered polarization and the Γ_1 representation indirectly from spectra containing both Γ_1 and Γ_{12} representations. For example, with the [110] orientation (Fig. 2)and XZ polarization, only contributions from the Γ_{12} irreducible representation are observed. With XY, XZ, YZ polarizations in the [100] orientation (Fig. 1) or XY, YZ polarizations in the [110] orientations, only the Γ_{15} irreducible representation contributes to the Raman spectrum. The Γ_1 contribution can be obtained by subtracting out the Γ_{12} contribution to the YY polarized

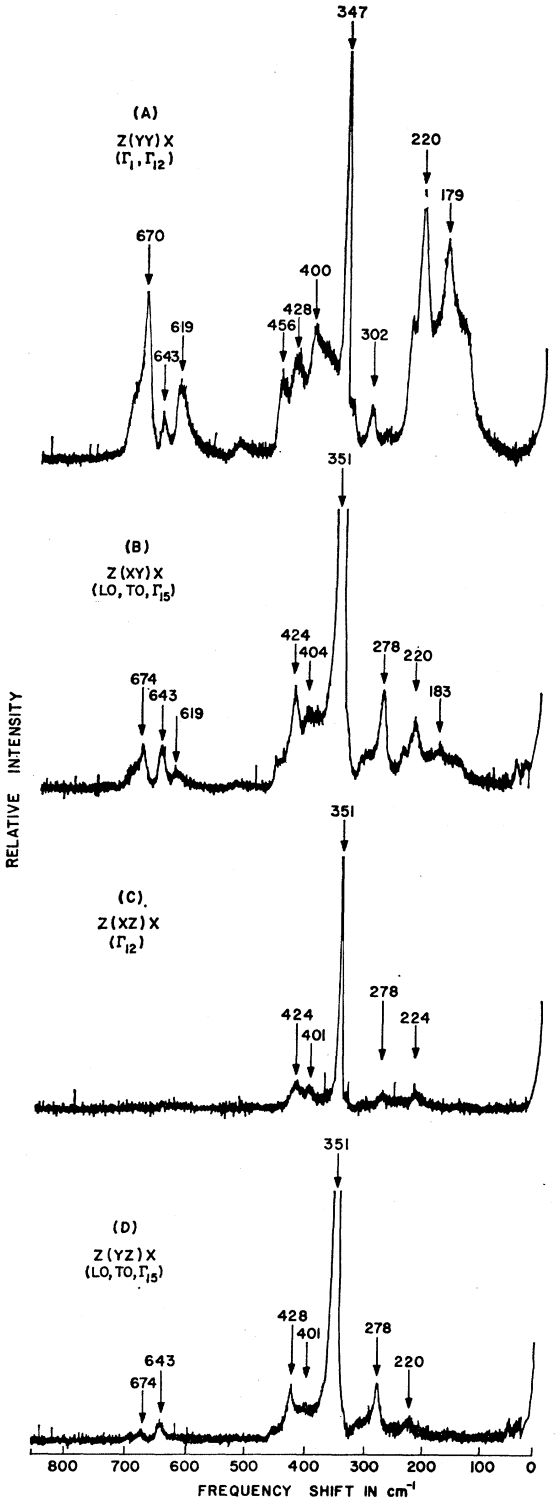

FIG. 2. Right-angle Raman scattering of cubic ZnS at room temperature and 4880-Å excitation. Two ⟨110⟩ crystallographic directions are along X and Z, and a ⟨100⟩ direction is along Y. The notation is the same as in Fig. 1.

spectra. A knowledge of the polarizability representations present in each second-order peak should give some indication as to which critical points in the Brillouin zone contribute to the second-order scattering and, in favorable cases, the symmetry species of the single-phonon states at these critical points. Indeed, it is this type of information which cannot be found directly from neutron diffraction measurements, but can be found, at least in principle, from the polarization characteristics of second-order Raman spectra. Two things impose limitations on this program. First, the optical quality of the sample is not very good so that the incident scattered light is depolarized slightly. This limits the precision of the polarization information obtainable from the Raman spectrum. In fact, it is the depolarizing effect of the sample which limits our ability to detect one particular irreducible representation of the polarizability in the presence of another rather than the sensitivity of the Raman instrument. Second, the two-phonon Raman spectra is undoubtedly a superposition of scattering from not only the critical points X, L, and W but also from other points on the Brillouin-zone boundary and points in the zone interior. The extent to which scattering from these other points contribute to the observed spectra is not known but we feel that the peaks are predominantly scattering from points X, L, and W.

EXPERIMENTAL

The experimental apparatus was described in detail in an earlier paper.[13] An argon-ion laser was used as the Raman source. Both 4880 and 5145 Å excitation was employed so that weak fluorescence could be distinguished from Raman spectra. The laser beam was focused in the sample with a 32-mm-focal-length microscope objective and the scattered light collected at 90°. A quartz lens was used to increase the total collection angle to 17°, and to match the scattered light into the $f/6.8$ optics of the in-tandem grating spectrometer. The scattered light was detected photoelectrically, the resulting signal amplified and recorded. The spectra were run at 25 Å/min with a 1-sec time constant and a spectral width of about 8 cm^{-1}. The polarization of the incident beam was varied with a half-wave plate and the polarization properties of the scattered light analyzed with a polaroid sheet placed in front of the entrance slit. The low-temperature experiments were done with the sample mounted in a helium cold-finger Dewar equipped with quartz windows.

Samples of cubic zinc sulphide were obtained as natural sphalerite from Juan Montal, Plaza Sagrando Corazon 1, Vilafranca del Pandes, Spain. They originated apparently[14] from the areas of Picos de Europa, Santander Province, Spain.

[13] W. G. Nilsen and J. G. Skinner, J. Chem. Phys. **47**, 1413 (1967).

[14] R. A. Laudise, E. D. Kolb, and J. P. DeNeufville, Am. Mineralogist **50**, 382 (1965).

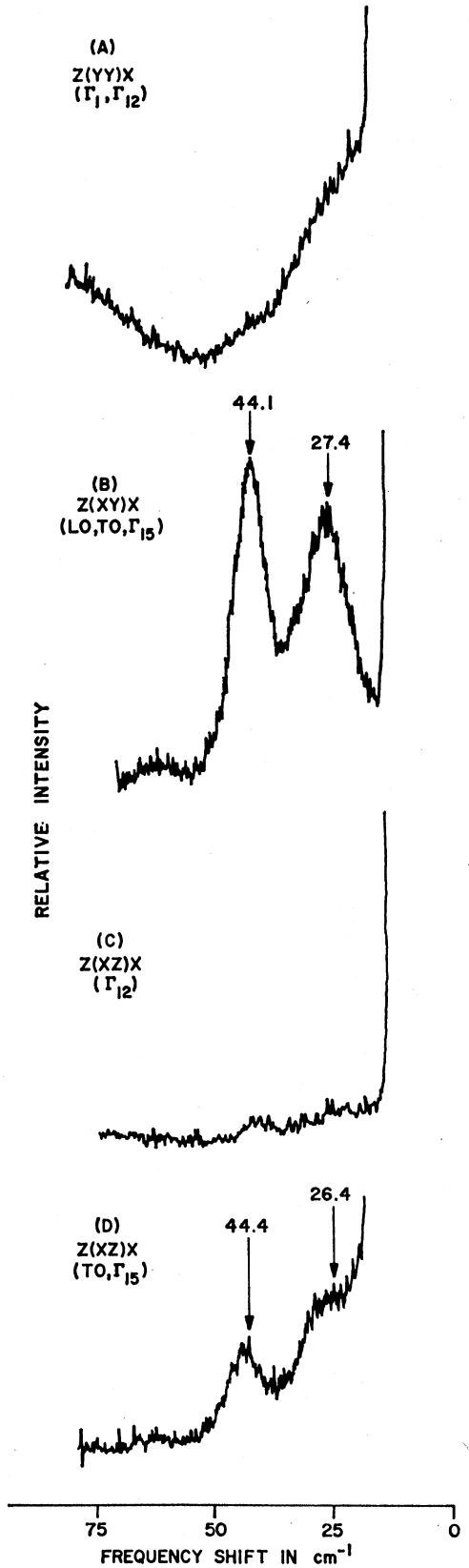

The samples were somewhat strained optically which caused some depolarization of the laser beam and scattered light. Also, reddish veins ran through the sample which were probably due to ferrous-ion impurity. Impurities also caused the sample to fluoresce slightly as can be seen in Fig. 1.

RESULTS

The Raman spectrum of cubic ZnS at room temperature is given in Figs. 1, 2, and 3 for right-angle scattering. The individual spectra are labeled with a series of four letters [for example, $Z(YY)X$ in spectrum A in Fig. 1]. These letters refer to the laboratory coordinate system defined above. The first and last letters are the directions of propagation of incident and scattered light, respectively, and the two letters in parentheses are the directions of polarization of the incident and scattered light. The spectra in Figs. 1 and 2 were measured with different crystal orientations; those in Fig. 1 with the $\langle 100\rangle$ directions along the X, Y, Z laboratory coordinate axes, those in Fig. 2 with $\langle 110\rangle$ crystallographic axes along X and Z and an $\langle 100\rangle$ axes along Y. Figure 3 shows some spectra close to the exciting line. These spectra were measured under conditions of greater sensitivity and resolution than in Figs. 1 and 2. The spectra in Figs. 3(A), 3(B), and 3(C) were taken with crystal orientation as in Fig. 2; Fig. 3(D) as in Fig. 1. The corresponding Raman intensity matrices for first-order scattering are given in the above section on crystal structure and selection rules. These matrices indicate that for the spectra in Fig. 1, the LO mode should appear in XY and YZ polarizations but not in YY or XZ polarizations. These selection rules are also summarized in the figures where we give the first-order modes (TO or LO) and irreducible representation of the polarizability which should appear in each individual spectrum. Actually, some depolarization of the laser beam occurs in the sample so that the LO line (at about 350 cm^{-1}) does appear in the YY and XZ polarizations but with weak intensity. In the allowed polarizations, the intensity of this Raman line is about 40 times greater than in the YY and XZ polarizations. For the spectra in Fig. 2, the depolarization effects were more pronounced, and the corresponding factor was about 7. Other spectra were taken with the same crystal orientation as in Fig. 2, but with much greater sensitivity, and these measurements gave depolarization factors of about 20. These factors represent the limit of our polarization information; that is, if a peak is Raman forbidden in a particular polarization, then its intensity should be reduced from that in an allowed polarization by a factor of about 40 for the spectra in Fig. 1 and

FIG. 3. Right-angle Raman scattering of cubic ZnS at room temperature and 4880-Å excitation near the exciting line. The spectra were run with more sensitivity (about seven times) and resolution than in Figs. 1 and 2. The A, B, and C spectra has the same crystal orientations as Fig. 2 and D, which was run with a smaller crystal, has crystal orientation as in Fig. 1.

TABLE II. Raman intensity versus temperature for the 44.1-cm^{-1} peak in cubic ZnS. The observed data are compared with those predicted for a first-order line with energy 44.1 cm^{-1}.

Temperature (°K)	Normalized intensities[a] Stokes line Observed	Stokes line Calculated[b]	Anti-Stokes line Observed	Anti-Stokes line Calculated[b]
300	1.0	1.0	0.80	0.81
220	0.82	0.79	0.57	0.58
197	0.60	0.70	0.45	0.53
175	0.56	0.62	0.42	0.45
142	0.47	0.55	0.29	0.36
84	0.29	0.36	0.16	0.17

[a] The observed and calculated intensities each have been normalized by dividing the results obtained at room temperature for the Stokes line into all of the data.

[b] Calculated for a first-order Raman line with energy 44.1 cm^{-1}. For the Stokes line, the intensity varies with temperature as $(1+n_j)$, for the anti-Stokes line as n_j. The results are again normalized by dividing through by the room-temperature value of $(1+n_j)$.

about 7 for Fig. 2. Many of our statements about Fig. 2, such as the absence of certain peaks in $Z(XZ)X$ polarization, actually reflect measurements made on the more sensitive spectra mentioned above where the depolarization factor was 20. Also, from the intensity matrices, the intensity of the TO line should be twice as great in the XZ polarization than the XY or YZ polarizations. The intensity ratio for YZ and XZ is 1.9. For XY and XZ polarizations, the observed intensities must be corrected for the fact that the spectrometer is more sensitive to Y-polarized light than Z-polarized light. With this correction, the intensity ratio for XY and XZ polarizations is 2.2 which is in resonable agreement with the predicted value of 2.0. In Fig. 2, the TO Raman line does not appear in XY polarization which is in agreement with the scattering matrix for this crystal orientation. We describe, at the end of this section, some additional spectra found very close to the laser line.

In addition to the above measurements, some relative and absolute intensity measurements were made on the LO and TO lines. The crystal orientation was the same as for the spectra in Fig. 1 and both XY and YZ polarizations were examined. The integrated intensity of the LO line was found to be a factor of 9.2 greater than that of the TO line at 4880 Å. This factor is probably reliable to about 20–30% and is independent of temperature from 300–30°K despite a marked reduction in the linewidth of the TO line on lowering the temperature. At 5145 Å, the ratio of integrated intensities for the LO and TO lines is nearly equal (8.9) to this ratio at 4880 Å but the individual heights and widths change somewhat.

The integrated intensity of the LO line was compared to that of the 992-cm^{-1} line of benzene at room temperature. The absolute cross section of this benzene line has been measured by a number of authors[15–18] and provides a convenient method of obtaining absolute Raman intensity data for a crystal. The benzene has an integrated intensity about 9.4 times greater than the LO line at 4880 Å and 8.2 times at 5145 Å.

Also, some intensity measurements were made as a function of temperature down to 30°K. It was observed that the intensity of the peaks in Fig. 1(A) decreased much more rapidly than the first-order LO and TO lines observed in the other polarizations. For first-order Stokes lines, the intensity should vary with temperature as $(1+n_i)$, where $n_i=(e^{E_i/kT}-1)^{-1}$ is the phonon-occupation number and the phonon energy E_i is equal to the observed energy shift of the Raman line. For second-order Stokes bands, the corresponding factor is $(1+n_i)(1+n_j)$ if both phonons are created (sum combination bands) and $(1+n_j)n_i$ if the lower-energy phonon is destroyed (difference combination bands). The energy shifts for second-order bands is either the sum or difference of the individual phonon energies E_i and E_j. More careful measurements were made on the 181, 222, 621, and 672 cm^{-1} bands in Fig. 1(A). The intensity of these bands decreased with decreasing temperature as expected for sum combination bands in which the individual phonon energies of each band are approximately equal. The intensity versus temperature relation is not particularly sensitive to the single-phonon energies and these quantities are determined more accurately by obtaining a consistent interpretation of the second-order spectrum and using the two-phonon energies derived from the energy shifts of the peaks in the spectrum. No evidence was found from these measurements that any of the bands in Fig. 1(A) were difference combination bands.

On careful examination of the spectra close to the exciting line, two more peaks were found. We show in the Discussion section that one of these peaks is composed of two difference combination bands on top of one another. These peaks can barely be seen in Figs. 1 and 2 but are easily detected when more sensitivity is used. In Fig. 3, we show on an expanded wavelength scale the Stokes part of the spectrum near the exciting line. Note that the top three spectra (A), (B), and (C) in Fig. 3 are for crystal orientation identical to that in Fig. 2 but the bottom spectrum (D) has crystal orientation as in Fig. 1. We call attention to the difficulty in determining if a particular peak is absent in a spectrum or merely covered over by intense Rayleigh scattering. Note particularly the 27.4 cm^{-1} peak in Figs. 3(B) and 3(D). In order to determine the origin of these peaks, rather careful measurements were made of their intensities as a function of temperature from 300–82°K. The integrated intensity of the LO line was used as an internal standard and it was assumed that the LO intensity varied with temperature as given above for a

[15] J. G. Skinner and W. G. Nilsen, J. Opt. Soc. Am. **58**, 113 (1968).

[16] F. J. McClung and D. Weiner, J. Opt. Soc. Am. **54**, 641 (1964); D. Weiner, S. E. Schwarz, and F. J. McClung, J. Appl. Phys. **36**, 2395 (1965).

[17] T. C. Damen, R. C. C. Leite, and S. P. S. Porto, Phys. Rev. Letters **14**, 9 (1965).

[18] G. Bret, Compt. Rend. **260**, 6362 (1965).

TABLE III. Raman intensity versus temperature data for the 27.4-cm^{-1} peak in cubic ZnS. The observed data are compared with those predicted for two difference combination bands.

Temperature (°K)	Normalized intensity[a] Stokes line Observed	Calculated[b] (LO-TO)	Calculated[b] (LA-TA)	Anti-Stokes line Observed	Calculated[b] (LO-TO)	Calculated[b] (LA-TA)
300	1.0	1.0	1.0	0.89	0.88	0.91
220	0.63	0.45	0.82	0.54	0.40	0.70
197	0.48	0.35	0.67	0.40	0.28	0.58
175	0.38	0.28	0.52	0.29	0.20	0.42
142	0.25	0.14	0.33	0.22	0.10	0.27
84	···	0.015	0.11	···	0.0095	0.076

[a] Since only relative intensities are of interest here, we normalized both observed and calculated data for ease of comparison. This normalization is done by dividing the observed intensity for the Stokes line at room temperature into the other observed intensity data and similarly for the calculated data.
[b] Calculated for the difference combination band $(E_j - E_i)$ where the phonon energy $E_j > E_i$. For the (LO-TO) band, $E_j = 333$ cm^{-1} and $E_i = 306$ cm^{-1}; for the (LA-TA) band, the energies are 110 and 88 cm^{-1}, respectively. The Raman intensity then varies as $n_i(1+n_j)$ for the Stokes peak and $n_j(1+n_i)$ for the anti-Stokes peak with $n_j = [\exp(E_j/kT) - 1]^{-1}$. The calculated numbers in the table are the values of $n_i(1+n_j)$ or $n_j(1+n_i)$ at the various temperatures divided by the value of $n_i(1+n_j)$ or $n_j(1+n_i)$ at room temperature.

first-order Raman line. For both 27.4 and 44.1 cm^{-1} peaks, the intensity of the anti-Stokes and Stokes lines obeys the Boltzmann distribution law quite closely which indicates that the peaks are actual Raman lines and not grating ghosts or fluorescence lines.

Some of the intensity versus temperature data for Stokes and anti-Stokes lines are summarized in Tables II and III. For convenience, the intensity data have been normalized so that the room-temperature Stokes intensity is made equal to one. In addition, some calculated intensities (also normalized in the same way) have been included in the tables for comparison. We discuss these data and calculations in the Discussion section.

DISCUSSION

First-Order Spectrum

The TO and LO modes near the zone center are located at 271 and 352 cm^{-1}. The identity of these modes is well established by their polarization characteristic as described in the Results section and by already published infrared[19] and Raman[1] studies. The Lyddane-Sachs-Teller[20] relation is well obeyed in cubic ZnS. This relation is given by $E_{LO}/E_{TO} = (\epsilon_0/\epsilon)^{1/2}$, where E_{LO} and E_{TO} are the energies of the LO and TO modes respectively near the zone center, ϵ_0 and ϵ are the low- and the high-frequency dielectric constant, and ϵ equals the square of the refractive index. The energy ratio is 1.30. If we take[21] $\epsilon_0 = 8.3$ and the index of refraction[22] at 5000 Å as 2.41, then the ratio $(\epsilon_0/\epsilon)^{1/2}$ becomes 1.20.

Of greater interest in connection with the first-order Raman lines is the relation between the line intensities and the linear electro-optic effect. This relation was first explained by Poulet[3] after it was discovered experimentally by Couture-Mathieu and Mathieu[1] that the intensity of the LO Raman line in zinc blende was much greater than the intensity of the TO line. This difference in intensity is due to the electric field caused by the polar lattice vibrations which provides an additional scattering mechanism for the Raman effect. In deriving the scattering cross sections for the TO and LO modes in zinc blende, Poulet[3] uses the local electric field produced by the polar phonons. In contrast, Loudon[7] adopts the view that the macroscopic electric field should be used in crystals where the electrons are not localized on individual atoms. The two electric fields are connected by the equation $E_{local} = E_{mac} + \frac{1}{3}4\pi P$ where P is the polarization. We shall adopt Loudon's viewpoint and attempt to derive the linear electro-optic coefficient from the Raman intensity measurements.

With this assumption, Loudon[7] derives expressions for the differential scattering efficiency caused by LO and TO phonons in the zinc-blende structure. He defines his differential scattering efficiency dS to be the ratio of scattered photons produced per unit time per unit cross sectional area of the crystal in the small solid angle $d\Omega$ about the direction of observation to the number of incident photons crossing unit area in unit time. His results were derived for unpolarized incident radiation and unanalyzed scattered radiation; that is, they refer to the sum of the YY, XY, XZ, and YZ polarizations shown in Fig. 1 and for which individual scattering matrix elements were derived above in the section on selection rules. Loudon's results for XY polarization would be

$$dS_i = \frac{Ld\Omega}{8c^4}\left|\frac{e^2(n_i+1)^{1/2}}{\hbar^{3/2}\omega_i^{1/2}m^2d}\left(\frac{V}{M}\right)^{1/2}R_{XY^Z}\right|^2$$

$$= \frac{Ld\Omega}{8c^4}|A_iR_{XY^Z}|^2$$

[19] C. Haas and J. P. Mathieu. J. Phys. Radium **15**, 492 (1954).
[20] R. H. Lyddane, R. G. Sachs, and E. Teller, Phys. Rev. **59**, 673 (1941).
[21] N. F. Mott and R. W. Gurney, *Electronic Processes in Ionic Crystals* (Dover Publications, Inc., New York, 1964), 2nd ed.
[22] S. J. Czysak, W. M. Baker, R. C. Crane, and J. B. Howe, J. Opt. Soc. Am. **47**, 240 (1957).

and for the LO mode

$$dS_l=\frac{Ld\Omega}{8c^4}\left|\frac{e^2(n_l+1)^{1/2}}{\hbar^{3/2}\omega_l^{1/2}m^2d}\left(\frac{V}{M}\right)^{1/2}R_{XY}{}^Z\right.$$
$$\left.-\frac{\hbar^{1/2}\omega_l^{1/2}(n_l+1)^{1/2}\omega_i{}^2\epsilon^2}{2\pi^{1/2}}\left(\frac{1}{\epsilon}-\frac{1}{\epsilon_0}\right)^{1/2}Z_{41}\right|^2$$
$$=\frac{Ld\Omega}{8c^4}|A_lR_{XY}{}^Z-BZ_{41}|^2.$$

In these expressions, L is the length of the scattering medium, $d\Omega$ is the small solid angle over which the scattered radiation is collected, c is the velocity of light, e and m are the electronic charge and mass, and d is the lattice constant of the crystal. The first term inside the absolute-value brackets in dS_t and dS_l are similar except that n_t and n_l refer to Bose-Einstein factors for TO and LO phonons and the parameters ω_t and ω_l are the phonon frequencies for the TO and LO modes. The quantities V and M are the volume and reduced mass of the crystal, ϵ_0 and ϵ are the low- and high-frequency dielectric constants, ω_i is the frequency of the incident radiation, and Z_{41} is the linear electro-optic constant in reduced notation.[23] The quantities A_l and A_t are connected by the relation

$$A_l=\left(\frac{(n_l+1)\omega_t}{(n_t+1)\omega_l}\right)^{1/2}A_t=0.84A_t.$$

There are two difficulties associated with determining Z_{41} from Raman intensity measurements. First, $R_{XY}{}^Z$ is not known except for its symmetry properties which are given by the scattering tensor. For this reason, we must determine not only the ratio of Raman intensities for the LO and TO modes but also the absolute differential scattering intensity for one of these modes. Second, the signs of Z_{41} and $R_{XY}{}^Z$ are not known.

In the absolute scattering intensity measurements made on benzene by Skinner and Nilsen,[15] the results were expressed in terms of a peak cross section σ_p rather than scattering efficiency. We first convert the former quantity into the latter quantity. In the terminology used in the above paper, the peak cross section is given by

$$\sigma_p=dP_R(\eta_R)/P_L(\eta_L)NLd\Omega.$$

In this equation, $dP_R(\eta_R)$ is the Raman power of wave number η_R scattered into the small solid angle $d\Omega$ toward the direction of observation, $P_L(\eta_L)$ is the incident power with wave number η_L, N is the number of molecules per unit volume, and L is the length of the scattering medium examined by the detector. For the 992 cm^{-1} line of benzene, Skinner and Nilsen[15] found $\sigma_p=1.05\times10^{29}$ cm^2/molecule sr cm^{-1} and the linewidth $\Delta\eta=2.3$ cm^{-1}. The total cross section for this line is obtained by integrating σ over the shape of the Raman line. For a Lorentzian line, this total cross section is given by $\sigma_p\Delta\eta\pi/2=3.8\times10^{-29}$ cm^2/molecule sr. This cross section can be converted into a scattering efficiency by multiplying it by the number of molecules/unit volume ($6.8\times10^{21}/cm^3$) and the power measurements converted to photons/unit time by taking proper account of the incident and scattered photon energy. The results are

$$dP_R(\eta_R)/(P_LLd\Omega)=\tfrac{1}{2}(\sigma_p\Delta\eta\pi)(N\eta_L/\eta_R)$$
$$=2.7\times10^{-7}/\text{cm sr}.$$

This quantity is equivalent to $dS/(Ld\Omega)$ given above in the notation of Loudon.

As mentioned above, the integrated power intensity measured for the 992 cm^{-1} line of benzene is 9.4 times greater than that of the LO line of ZnS and 86 times greater than that of the TO line. Two corrections are needed before these results can be used to derive scattering efficiencies. First, the solid angle of collection is proportional to the square of the refractive index so that the above numbers should be increased by a factor of $(2.41/1.50)^2=2.59$. Second, there is a small correction to convert power measurements into photons/unit time. With these corrections, we find $dS_t/(Ld\Omega)=11.8\times10^{-10}$/cm and $|A_tR_{XY}{}^Z|=8.8\times10^{16}$ $cm^{3/2}$ sec^{-2}. For the longitudinal mode, $A_lR_{XY}{}^Z=7.4\times10^{16}$ $cm^{3/2}$ sec^{-2} and $dS_l/(Ld\Omega)=10.7\times10^{-9}$/cm so that $|BZ_{41}|$ is equal to 19×10^{16} or 34×10^{16} $cm^{3/2}$ sec^{-2} depending on the relative signs of Z_{41} and $R_{XY}{}^Z$. These measurements yield an electro-optic coefficient $|Z_{14}|$ of 2.0×10^{-8} or 3.5×10^{-8} cm/statV, again depending on the signs of Z_{41} and $R_{XY}{}^Z$. The value of $|Z_{41}|$ measured electro-optically is[24,25] 5×10^{-8} cm/statV at 4900 Å. These two quantities are not exactly equivalent since the Z_{41} from Raman measurements contains only the electronic or high-frequency part of the electro-optic effect whereas the electro-optical measurements were made statistically and contain both mechanical and electronic contributions. The mechanical or low-frequency part of Z_{41} is equal to $P_{44}d_{14}=1.3\times10^{-8}$ cm/statV, where P_{44} is the electro-optic constant obtained from Ref. 24 and d_{14} is the piezoelectric constant from Ref. 26. Again, the relative signs are not known but if the mechanical and electronic parts have the same sign, then Z_{41} (electronic) $=3.7\times10^{-8}$ cm/statV.[27] This close agreement should be regarded as largely accidental since the absolute intensity measurements are nowhere

[23] J. F. Nye, *Physical Properties of Crystals* (Oxford University Press, London, 1960).

[24] S. Namba, J. Opt. Soc. Am. **51**, 76 (1961).

[25] R. Bechmann, J. Phys. Chem. Solids **16**, 100 (1960).

[26] *American Institute of Physics Handbook* (McGraw-Hill Book Co., New York, 1963), 2nd ed.

[27] Even after subtracting out the mechanical effects in the electro-optic effect, the Raman and electrically measured coefficients do not correspond exactly. The Raman electro-optic coefficient includes only the motion of the electron clouds whereas the coefficients measured electrically (without mechanical effects) includes in addition some effects due to the motion of the atomic nuclei. Since the static and optical dielectric constants are not very different, it is unlikely that the two electro-optic constants are significantly different.

near this accurate. Also, there is another severe limitation to the accuracy and reliability of our measurement connected with the fact that suitable cubic ZnS samples are found only in nature. The various electro-optic, refractive index and Raman measurements were made on different samples originating from different parts of the world and undoubtedly containing different amounts of impurity. Indeed, the electro-optic coefficient is known[25] to vary from sample to sample. Thus, the index of refraction and electro-optic coefficient obtained from the literature are not necessarily accurate for the sample used for our Raman measurements. Also, these measurements point up the importance of knowing the signs of Z_{41} and $R_{XY}{}^{Z}$. Since $P_{44}d_{14}$ is positive, we obtain our best agreement with Z_{14} (electronic) positive and $R_{XY}{}^{Z}$ positive but the measurements are probably not sufficiently reliable to put much confidence in these conclusions.

Absolute-intensity measurements were also made using 5145-Å excitation. Under these conditions, the integrated intensity of the benzene line was only 8.2 times greater than the LO line of ZnS. The ratio of integrated intensity for the LO and TO modes was 8.9, in close agreement with the results at 4880 Å even though the heights and widths changed considerably. These measurements yield an electro-optic coefficient Z_{41} of 4.3×10^{-8} or 2.4×10^{-8} cm/statV, depending on the relative signs of Z_{41} and $R_{XY}{}^{Z}$. The electro-optic coefficient of cubic ZnS is known to increase in absolute value with increasing wavelength[24,25] in agreement with the trend shown here.

In addition to the expected LO and TO Raman lines described above, one other weak first-order line was found near the exciting line at 44.1 cm^{-1}. Obviously, this line cannot be scattering from the ordinary optical modes since the LO and TO lines account for all the possible optical modes in the zinc-blende structure and, not from the acoustic modes since they are located much closer to the exciting line. To eliminate the possibility that this peak is a difference combination band, its intensity was measured as a function of temperature as described above. The results are summarized in Table II together with the calculated intensities for a first-order line with energy 44.1 cm^{-1}. Both the observed and calculated intensities have been normalized so that the observed and calculated results are equal to one for the Stokes line at 300°K. As can be seen from a comparison of observed and calculated intensities, the peak at 44.1 cm^{-1} is due to first-order Raman scattering. A difference combination band would yield a vastly different dependence of Raman intensity on temperature and a sum combination band or overtone band at such a low energy seems impossible. The polarization properties of this Raman line may be summarized as follows: It is absent under polarization conditions equivalent to Figs. 1(A), 2(A) [shown in Fig. 3(A)], and Fig. 2(C) [shown in Fig. 3(C)]. It is present under polarization conditions equivalent to Figs. 1(B), 1(C) [shown in Fig. 3(D)], 1(D), and 2(B) [shown in Fig. 3(B)]. The polarization characteristics of this mode seems to parallel that of the TO Raman line. Although the origin of the Raman line at 44.1 cm^{-1} is not definitely established from these measurements, it appears to be some sort of local mode caused by impurities in our sample of cubic ZnS. A significantly purer sample was not available to test this conjecture.

TABLE IV. Phonon branch assignments for the first- and second-order Raman spectrum of cubic ZnS.

Observed energy shift[a] (cm^{-1})	Assignment	Observed polarization characteristics	Calculated energy shift[b] (cm^{-1})
27.4	LA-TA	Γ_{15}	22
	LO-TO	Γ_{15}	27
44.1	local mode	like the TO mode	
176	2 (TA)	Γ_1	176
219	2 (LA)	$\Gamma_1,\Gamma_{12},\Gamma_{15}$	219
271	TO		271
295	2(0) at W	Γ_1	
352	LO		352
386	TO+TA	$\Gamma_1,\Gamma_{12},\Gamma_{15}$	394
422	TO+LA	$\Gamma_1,\Gamma_{12},\Gamma_{15}$	416
	LO+TA	$\Gamma_1,\Gamma_{12},\Gamma_{15}$	421
448	LO+LA	Γ_1	443
511	2(0) at W	Γ_1	
612	2 (TO)	Γ_1,Γ_{15}	612
636	LO+TO	Γ_1,Γ_{15}	639
665	2 (LO)	Γ_1,Γ_{15}	665

[a] These values were determined by superimposing the Raman spectrum on the spectrum of a He-Ne discharge. The energy shifts given in this table are probably accurate to ±2 cm^{-1} for narrow lines and less accurate for the broader, weaker lines. The numbers in Figs. 1 and 2 are probably accurate to ±6 or 8 cm^{-1}, depending on line intensity and width.

[b] Assuming the following at the Brillouin-zone boundary (X): TA = 88 cm^{-1}, LA = 110 cm^{-1}, TO = 306 cm^{-1}, and LO = 333 cm^{-1}. These values are taken from the corresponding overtones shown in Fig. 1. At the zone center (Γ), the energy of the TO and LO modes are taken from our own data.

Second-Order Spectrum

Before discussing the second-order spectrum in detail, we outline certain assumptions we have made in interpreting the origin of the peaks. First of all, cubic ZnS is highly ionic or polar compared to say GaP and GaAs which also have the zinc-blende structure. For this reason, we assume that the phonon branches do not cross in the Brillouin zone at least along the [001] and [111] directions. Such level crossing does occur in less ionic crystals. Also, we assume that the most intense scattering comes from critical points X and L since they have the highest symmetry and greatest degeneracy on the zone boundary. The ionic character of cubic ZnS makes it likely that the same phonon branch has nearly the same energy (to within 20–40 cm^{-1}) at X as at L since at these critical points, the phonon modes are purely transverse or longitudinal. At critical point W, the phonons are not pure transverse or longitudinal.

We give first a general interpretation of the second-order spectrum in terms of the phonon energies at the zone boundary. The strongest peaks appear in (YY) polarization in the two crystal orientations examined. In identifying peaks, we use the energy shifts given in Table IV. The peak at 176 cm^{-1} is the TA overtone and

the one at 219 cm^{-1} is the LA overtone. The (TA+LA) band should be at 198 cm^{-1} but is not observed probably because it has weak intensity and is covered over by the more intense TA and LA overtones. The TO and LO overtones are found at 612 cm^{-1} and 665 cm^{-1}, respectively, and the sum combination band (TO+LO) is found at 636 cm^{-1}. If we derive the single phonon energies at the zone boundary from the overtone bands, then the (TO+LO) band should be at 639 cm^{-1}.

It is of importance to establish that combination bands exist between the phonons causing the overtones at 176 and 219 cm^{-1} as well as the overtones at 612 and 665 cm^{-1}. If such combinations exist, these overtones must originate from different phonon branches as is supposed above rather than the same branch at different points in the Brillouin zone. In the latter case, combinations are not allowed since momentum is not conserved. Difference combination bands are more easily identified than sum bands since their intensities vary with temperature in a way which is distinct from overtones and first-order lines located in the same part of the spectrum. For this reason, we investigated the part of the spectrum near the exciting line under conditions of greater sensitivity (about seven times greater than in Figs. 1 and 2) and greater resolution. The results are given in Fig. 3. We interpret the band at 27.4 cm^{-1} as a superposition of the two difference bands (LO-TO) and (LA-TA). In order to show this conclusively, we measure the intensity of this band as a function of temperature. The results are given in Table III together with the variation of Raman intensity with temperature predicted for the difference bands (LO-TO) and (LA-TA). The data and calculations have been normalized so that the intensity of the Stokes line is made equal to one at room temperature. They show that the peak at 27.4 cm^{-1} is a difference combination band. Only the (LO-TO) and (LA-TA) difference band are likely to be located in this part of the spectrum. A comparison of the observed and calculated intensity versus temperature relation shown in Table III indicates that both the (LO-TO) and (LA-TA) bands are superimposed in the peak at 27.4 cm^{-1}. We note that the (LA+TA) sum band is not observed probably because it is covered over by the much more intense LA and TA overtones and the corresponding difference band is the only source of polarization information concerning this combination band.

From the overtone energies, we derive the one-phonon energies at the zone boundary as 88, 110, 306, and 333 cm^{-1} for the TA, LA, TO, and LO modes, respectively. We do not attempt to distinguish between phonon energies at X and L although we would guess that the small shoulders below 2 TA (at 150 cm^{-1}) and above 2 LA (at 240 cm^{-1}) are from point X and the peaks from point L. Similarly for the shoulders from below 2 TO and above 2 LO. We should see the sum combination bands (LO+LA) and (TO+TA) at 443 and 394 cm^{-1} and these peaks are found reasonably close to these energies (see Table IV). The sum bands (TO+LA) and (LO+TA) should be found at 416 and 421 cm^{-1} and a peak is seen at 422 cm^{-1}.

The origin of the peaks at 295 and 511 cm^{-1} has not been well established. From temperature dependence measurements, it is known that they are not difference combination bands. They are found only in (YY) polarization for the two crystal orientations. It is unlikely that they are three-phonon peaks since such Raman processes should yield much less intense peaks. It is more likely that they are two-phonon peaks which originate from other parts of the Brillouin zone, either other critical points on the zone boundary or from a high-symmetry point inside the zone. Our best guess is that they are overtone bands originating from the W critical point on the zone boundary where the single-phonon energies might deviate somewhat from those at the X and L critical points.

The intensity-versus-temperature measurements on the part of the spectrum shown in Fig. 1 did not indicate the presence of any difference combination bands in addition to the (LA-TA) and (LO-TO) shown in Fig. 3. This is not surprising since their intensities would be quite weak and they would overlap with the more intense sum and overtone bands. For example, the (TO-TA) and (LO-LA) bands should be located at 218 cm^{-1} and 223 cm^{-1}. However, their intensities should be quite weak, in fact reduced by a factor of approximately two from the already weak sum bands, and they are located in the same part of the spectrum as the intense LA overtone. A similar statement can be made about the (LO-TA) and (TO-LA) bands.

A more precise discussion of the second-order spectrum can be made by considering the polarization properties of the spectrum. We discuss these polarization properties in terms of the irreducible representations of the polarizability tensors Γ_1, Γ_{12}, and Γ_{15}. Our aim is to determine from our observed spectra which of these representations are present in each peak and compare these results with those predicted from crystal symmetry (Table I). Our motivation for doing this is twofold. First, we would like to obtain more evidence to substantiate our assignments made above. Second, we would like to determine the critical points from which the dominant part of the two-phonon scattering originates. In favorable cases, such knowledge might lead to information about the symmetry species of the single-phonon states at certain points in the Brillouin zone. Indeed, it is this latter information which is not directly accessible from neutron-diffraction experiments.

The strongest and largest number of lines in the second-order spectrum of cubic ZnS contain polarization symmetry Γ_1. This can be seen from the (YY) polarization in Figs. 1(A) and 2(A) which admits both Γ_1 and Γ_{12} representations and from the absence of strong

spectra in (XZ) polarization of Fig. 2(C) which admits only Γ_{12} representations. The predominance of Γ_1 symmetry in the second-order spectra is not surprising in view of the selection rules given in Table I. Also, the intensity of scattering seems to be strongest for the Γ_1 representation. We note that the absence of a particular polarization representation in a peak is not necessarily significant since it may be due to weak scattering intensity rather than selection rules. The presence of a particular representation is obviously more significant information. For example, we were not able to detect any Γ_{12} spectra in the LO and TO overtones even when the sensitivity was increased to where peaks could be detected due to depolarization effects. But the derived selection rules (Table I) indicate that Γ_{12} should be present in both overtones at critical point X and in the TO overtone at point L. If the absence of Γ_{12} in the LO and TO overtones was due to selection rules, then the scattering could not originate from either critical point X or L which is very unlikely. More significant is the presence of Γ_{15} in both of these overtones with an intensity of about 1/7 that of the Γ_1 spectra in both cases. Since in the calculated selection rules, Γ_{15} is absent for the LO overtone at point X and for the TO overtone at point L, then the scattering cannot originate from just one of these critical points alone. In other words, the second-order scattering originates from more than one point on the Brillouin-zone boundary. We again point out that the limit of our sensitivity with regard to detecting the presence of a particular polarization representation is determined by depolarization effects in the sample rather than the sensitivity of our instrument.

The acoustic overtones also yield polarization information. For example, the LA overtone contains both Γ_{12} and Γ_{15} with about equal intensity and Γ_1 with about five times the intensity of Γ_{12} and Γ_{15}. The TA overtone contains Γ_1 but not Γ_{12} nor Γ_{15}. The difference in the observed polarization properties of the TA and LA overtones is not surprising in view of the different symmetry species for these modes both at critical point X and L. More surprising is the different observed polarization properties of the TA and TO overtones since these modes have the same symmetry species at both L and X. The LO and LA modes have identical symmetry species at L but different symmetry species, although still identical selection rules, at critical point X. It seems that the observed polarization properties of the overtone bands can be accounted for by the selection rules at critical points X and L although some allowed polarization representations are too weak to be detected.

A comparison of the observed and calculated polarization properties of the combination bands lead to somewhat more puzzling results than in the case of the overtone bands. Those combination bands which originated from like-polarized phonon modes gave results consistent with the derived selection rules for critical points X and L; those from differently-polarized modes yielded polarizations not predicted by these selection rules. For example, the (LO+LA) band showed only Γ_1 polarization whereas the selection rules predict both Γ_1 and Γ_{15} at L and only Γ_{15} at X. Here again, though, the Γ_{15} spectra is probably too weak to be detected especially as it is quite close to other fairly intense bands. The (TO+LA) band contains not only Γ_1 but also Γ_{12} and Γ_{15} which is in agreement with the selection rules at X and L.

In contrast, the combination bands arising from differently-polarized phonon modes should not show any Γ_1 polarized spectra for scattering which originates from critical points X and L. But some of these combination bands do show some Γ_1 polarized spectra. For example, the (LO+TO) band at 636 cm^{-1} is present in Figs. 1(A) and 2(A) but not in Fig. 2(C), which indicates Γ_1 polarized spectra. The corresponding difference combination band (LO-TO) does not seem to show Γ_1 polarization (Fig. 3), although some overlap with the Rayleigh scattering and the fact that two difference bands (LO-TO) and (LA-TA) occur at the 27.4 cm^{-1} peak makes firm conclusions about the presence of (LO-TO) in Fig. 3(A) difficult. Obviously, the sum and difference bands (LO$\pm$TO) should show the same polarization properties. Possibly, the inconsistency is due to two bands being superimposed at 636 cm^{-1}, one the sum band mentioned above and the other an optical-mode overtone from another point (say, critical point W) in the Brillouin zone. Both of the difference bands show Γ_{15} spectra [Figs. 2(B) and 3(B)] but not Γ_{12} spectra [Figs. 2(C) and 3(C)]. The two bands (TO+LA) and (LO+TA) located at 422 cm^{-1} also shows some indication of Γ_1 spectra in that its intensity appears greater in (YY) polarization [Fig. 2(A)] than (XZ) polarization [Fig. 2(c)] but in this case the overlap with neighboring peaks is so extensive as to make firm conclusions based on intensities in each polarization impossible. These bands do contain Γ_{15} and Γ_{12} in agreement with the selection rules. The difference band (LA-TA) shows only Γ_{15} spectra which is not in violation of the selection rules at X and L. We note in passing that the LO and LA modes cannot be assigned to symmetry species X_1 or X_3 by two-phonon Raman measurements since the selection rules (polarization representations) are identical. The peaks at 295 and 511 cm^{-1} show only Γ_1 polarization which is in agreement with the selection rules for overtones at critical point W.

CONCLUSIONS

The Raman spectrum of cubic ZnS is well worth studying because of its relatively simple crystal structure. This makes it possible to test much more directly and unambiguously theoretical models connecting the lattice dynamics of a crystal and some of its bulk

properties. As a trivial example, the optical-mode energies near the Brillouin-zone center are related to the low- and high-frequency dielectric constant by the Lyddane-Sachs-Teller equation. The predicted and observed relationship agree quite closely in cubic ZnS. More interesting is the fact that the linear electro-optic constant can be predicted reasonably accurately from the Raman intensities of the LO and TO modes using a relation due to Loudon.[7] The close agreement between the linear electro-optic constant obtained from Raman intensities and by direct measurement makes it likely that the macroscopic rather than the local electric field produced by polar phonons is the appropriate one to use in calculations involving semiconducting crystals.

The simple crystal structure of cubic ZnS also makes it possible to obtain a reliable interpretation of the second-order Raman spectra exhibited by this crystal. From this interpretation, we find the single-phonon energies at the Brillouin-zone boundary as follows: TA=88 cm^{-1}, LA=110 cm^{-1}, TO=306 cm^{-1}, and LO=333 cm^{-1}. These values represent some sort of averages at the zone boundary with X and L critical points being weighted most heavily.

The selection rules derived for the second-order Raman effect in the zinc-blende structure at the critical points L and X on the zone boundary were compared with the observed polarization properties of the Raman spectra. In general, the agreement between calculated and observed selection rules is quite good. These selection rules are most conveniently described in terms of the irreducible representations of the polarizability allowed for the T_d point group. The selection rules predict an abundance of Γ_1 spectra and this polarizability representation is found to dominate the observed spectra both in the number of peaks exhibiting this polarization characteristic and the intensity of the peaks. In no case was the Γ_1 polarizability representation absent in a peak where its presence was predicted from symmetry considerations. The intensities of the Γ_{12} and Γ_{15} spectra were for the most part much weaker than the Γ_1 spectra and in some cases was not detected although allowed by symmetry. Also, the presence of both Γ_{12} and Γ_{15} representations in certain peaks in which only one of these representations is allowed at critical point X and one at L indicates that scattering from both of these critical points contributes significantly to the observed spectra. For some combination bands involving differently-polarized phonons, Γ_1 spectra is observed even though not allowed at critical points X, L, or W. This result is not firmly established since in one case the corresponding difference combination band did not show any Γ_1 polarization and in the other cases, overlap with adjacent peaks made it difficult to distinguish between Γ_1 and Γ_{12} spectra. This result might indicate that some second-order spectra is detected from parts of the Brillouin zone other than the above critical points or that the selection rules do not hold precisely because the wave vectors of the individual phonons are not exactly of equal magnitude and opposite direction.

Some general remarks concerning the value of the second-order Raman effect in deriving information on the lattice dynamics of a crystal is perhaps in order at this point. Second-order Raman spectra, even under the most favorable conditions, does not give as detailed information on phonon energy as a function of wave vector and crystal direction as does neutron diffraction. In cases like cubic ZnS where available crystals are too small for reliable neutron diffraction work, second-order Raman measurements probably provide the most reliable source of phonon energy data near the Brillouin-zone boundary. Also, in favorable cases such as ZnS and SiC, the existence of other crystal modifications makes it possible to obtain information on phonon energies inside the Brillouin zone from the first-order Raman spectra of the modified crystal. Ideally, neutron diffraction and second-order Raman spectra should supplement one another. The former gives quite detailed information on phonon energies in various parts of the Brillouin zone. The latter gives information, through the polarization characteristics of the spectra, on the symmetry species of the phonon modes at scattering points in the Brillouin zone. With neutron diffraction, various phonon directions and wave vectors can be separated out for individual study but relatively large single crystals of good quality are required. With second-order Raman effect, no such selection can be made and the spectra represent a superposition of scattering from various phonon directions and wave vectors each weighted differently. Thus, it is much more difficult to interpret and obtain reliable information from second-order Raman spectra than neutron diffraction data but measurements can be made on much smaller single crystals.

ACKNOWLEDGMENTS

The author wishes to thank J. R. Potopowicz for technical assistance in connection with the spectroscopy measurements and S. Singh, S. H. Wemple, and J. G. Skinner for discussions in regard to various aspects of this work.